



Gearbox Reliability Collaborative High-Speed Shaft Calibration

J. Keller
National Renewable Energy Laboratory

B. McNiff
McNiff Light Industry

**NREL is a national laboratory of the U.S. Department of Energy
Office of Energy Efficiency & Renewable Energy
Operated by the Alliance for Sustainable Energy, LLC**

This report is available at no cost from the National Renewable Energy Laboratory (NREL) at www.nrel.gov/publications.

Technical Report
NREL/TP-5000-62373
September 2014

Contract No. DE-AC36-08GO28308

Gearbox Reliability Collaborative High-Speed Shaft Calibration

J. Keller

National Renewable Energy Laboratory

B. McNiff

McNiff Light Industry

Prepared under Task No. WE14.3A01

**NREL is a national laboratory of the U.S. Department of Energy
Office of Energy Efficiency & Renewable Energy
Operated by the Alliance for Sustainable Energy, LLC**

This report is available at no cost from the National Renewable Energy Laboratory (NREL) at www.nrel.gov/publications.

NOTICE

This report was prepared as an account of work sponsored by an agency of the United States government. Neither the United States government nor any agency thereof, nor any of their employees, makes any warranty, express or implied, or assumes any legal liability or responsibility for the accuracy, completeness, or usefulness of any information, apparatus, product, or process disclosed, or represents that its use would not infringe privately owned rights. Reference herein to any specific commercial product, process, or service by trade name, trademark, manufacturer, or otherwise does not necessarily constitute or imply its endorsement, recommendation, or favoring by the United States government or any agency thereof. The views and opinions of authors expressed herein do not necessarily state or reflect those of the United States government or any agency thereof.

This report is available at no cost from the National Renewable Energy Laboratory (NREL) at www.nrel.gov/publications.

Available electronically at <http://www.osti.gov/scitech>

Available for a processing fee to U.S. Department of Energy and its contractors, in paper, from:

U.S. Department of Energy
Office of Scientific and Technical Information
P.O. Box 62
Oak Ridge, TN 37831-0062
phone: 865.576.8401
fax: 865.576.5728
email: <mailto:reports@adonis.osti.gov>

Available for sale to the public, in paper, from:

U.S. Department of Commerce
National Technical Information Service
5285 Port Royal Road
Springfield, VA 22161
phone: 800.553.6847
fax: 703.605.6900
email: orders@ntis.fedworld.gov
online ordering: <http://www.ntis.gov/help/ordermethods.aspx>

Cover Photos: (left to right) photo by Pat Corkery, NREL 16416, photo from SunEdison, NREL 17423, photo by Pat Corkery, NREL 16560, photo by Dennis Schroeder, NREL 17613, photo by Dean Armstrong, NREL 17436, photo by Pat Corkery, NREL 17721.

Acknowledgments

This work was supported by the U.S. Department of Energy under contract number DE-AC36-08GO28308 with the National Renewable Energy Laboratory.

List of Abbreviations and Acronyms

| | |
|-------|--------------------------------------|
| CRB | cylindrical roller bearing |
| DAS | data acquisition system |
| deg | degree |
| Fcal | Calibration force |
| ft-lb | foot-pound |
| GB | gearbox |
| GPa | gigapascal |
| GRC | Gearbox Reliability Collaborative |
| HS | high speed |
| HSS | high-speed shaft |
| Hz | hertz |
| kg | kilogram |
| kN | kilonewton |
| kNm | kilonewton-meter |
| kW | kilowatt |
| lb | pound |
| m | meter |
| Mcal | Calibration moment |
| mV/V | millivolts per volt |
| MW | megawatt |
| NI | National Instruments |
| NREL | National Renewable Energy Laboratory |
| NWTC | National Wind Technology Center |
| STBD | starboard |
| TRB | tapered roller bearing |
| V | volt |
| V/V | volts per volt |

Nomenclature

| | |
|----------------|----------------------------|
| d | inner diameter of shaft |
| D | outer diameter of shaft |
| $\frac{dV}{V}$ | strain gauge output |
| E | elastic modulus |
| G | shear modulus |
| G_F | strain gauge factor |
| I | area moment of inertia |
| J | polar moment of inertia |
| K_M | bending moment coefficient |
| K_T | torque coefficient |
| M | bending moment |
| T | torque |
| ε | bending strain |
| γ | shear strain |
| ν | Poisson's ratio |
| σ | bending stress |
| τ | shear stress |

Table of Contents

| | | |
|----------|--|-----------|
| 1 | Introduction | 1 |
| 2 | High-Speed Shaft Test Article | 2 |
| | 2.1 Description and Modifications..... | 2 |
| | 2.2 Installation..... | 2 |
| | 2.3 Instrumentation..... | 4 |
| | 2.4 Calibration Requirements..... | 10 |
| 3 | Test Configuration | 11 |
| | 3.1 Arrangement..... | 11 |
| | 3.2 Load Application..... | 11 |
| | 3.3 Data Collection..... | 12 |
| 4 | Data Analysis | 13 |
| | 4.1 Response Verification..... | 13 |
| | 4.2 Calibration..... | 15 |
| | 4.2.1 Bending Moment Coefficient Derivation..... | 15 |
| | 4.2.2 Torque Coefficient Derivation..... | 15 |
| | 4.2.3 HSS Calibration Coefficients..... | 16 |
| | 4.2.4 Calibration Results..... | 16 |
| | 4.3 Final Calibration Coefficients..... | 18 |
| 5 | Conclusions | 22 |
| 6 | References | 23 |

List of Figures

| | |
|--|----|
| Figure 1. Schematic of HSS installation in the gearbox. <i>Illustration from Powertrain Engineers Inc.</i> | 2 |
| Figure 2. The effect of the deep counter bore in the HSS housing..... | 4 |
| Figure 3. HSS pinion face width load distribution. <i>Illustration from McNiff Light Industry</i> | 6 |
| Figure 4. HSS bending upwind of the pinion. <i>Illustration from McNiff Light Industry</i> | 7 |
| Figure 5. HSS bending downwind of the pinion. <i>Illustration from McNiff Light Industry</i> | 8 |
| Figure 6. HSS bending and torque downwind of the TRB pair. <i>Illustration by McNiff Light Industry</i> | 9 |
| Figure 7. HSS torque, bending, and pinion strain gauges. <i>Photos by Scott Naucner, NREL 30252, 30250, and 30251 (from left to right)</i> | 10 |
| Figure 8. Instrumented HSS assembly. <i>Photo by Jonathan Keller, NREL 27895</i> | 10 |
| Figure 9. Shaft bending moment application. <i>Illustration from McNiff Light Industry</i> | 11 |
| Figure 10. Shaft torque application. <i>Illustration from McNiff Light Industry</i> | 12 |
| Figure 11. Y-axis gauge response to y-axis moment (top), z-axis moment (left) and torque (right) | 13 |
| Figure 12. Z-axis gauge response to z-axis moment (top), y-axis moment (left), and torque (right) | 14 |
| Figure 13. Torque gauge response to torque (top), to y-axis moment (left), and z-axis moment (right) | 14 |
| Figure 14. Bending moment diagram..... | 17 |
| Figure 15. Measured bending moments in dynamometer test..... | 20 |
| Figure 16. Measured torque in dynamometer test..... | 21 |

List of Tables

| | |
|---|----|
| Table 1. HSS Instrumentation | 5 |
| Table 2. HSS Properties..... | 16 |
| Table 3. Final HSS Calibration Coefficients | 18 |

1 Introduction

In the National Renewable Energy Laboratory (NREL) Gearbox Reliability Collaborative (GRC) project, engineers investigate gearbox reliability primarily through testing and modeling to validate the design process. Previous dynamometer testing focused on acquiring measurements in the planetary section of the test gearbox [1]. Before these tests were conducted, the strain gauges installed on the planetary cylindrical roller bearings and high speed shaft tapered roller bearings were calibrated in a load frame [2,3].

Recent input from GRC participants has highlighted the need for measurements of gear and bearing responses—including reactions, load distributions, and temperatures in the high-speed (HS) section of the gearbox—because of a high rate of failures in the locating bearings supporting the high-speed shaft (HSS) [4]. Consequently, instrumentation has been added to the HSS, pinion, and tapered roller bearing (TRB) pair of the GRC gearbox (GB) #2 to measure loads and temperatures. In a portion of the GRC dynamometer test program, these loads are being measured in test conditions, including normal operation, generator radial misalignment, and simulated emergency stop conditions [4].

The new HSS bending moment and torque instrumentation was calibrated on November 26, 2013, before the planned dynamometer tests began. The purpose of this document is to describe this calibration process and results. This will allow the raw shaft bending and torque signals collected during subsequent dynamometer testing to be converted to the proper engineering units and coordinate system reference for comparison to design loads and simulation model predictions.

2 High-Speed Shaft Test Article

2.1 Description and Modifications

In operation, the HSS is supported on its upwind end by a cylindrical roller bearing (CRB) and near its midpoint by a close-coupled TRB pair. The TRB pair is mounted in an O-configuration, which provides greater tilting stiffness than an X-configuration. Figure 1 shows the entire HSS assembly and gearbox housing.

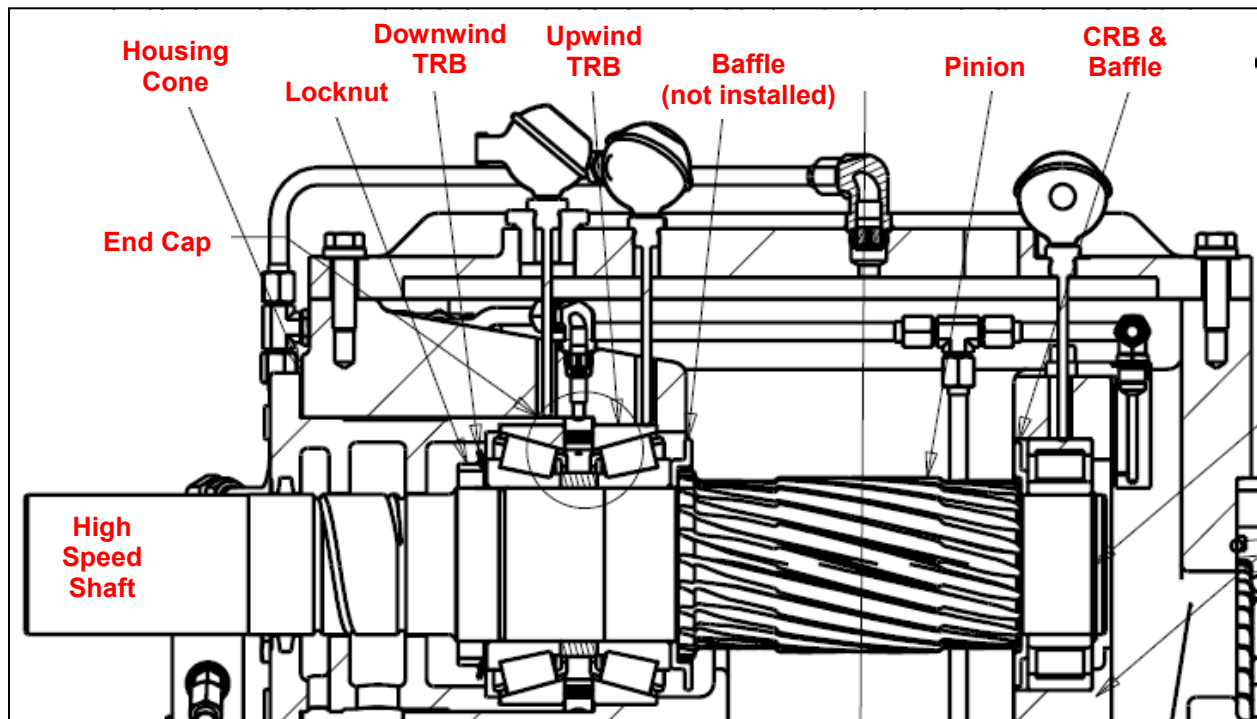


Figure 1. Schematic of HSS installation in the gearbox. Illustration from Powertrain Engineers Inc.

The original HSS (P/N 251244) was removed from GB #2 in November 2012. It was then modified (P/N 254623) in early 2013 to accommodate the instrumentation itself. The most significant modifications were the removal of 35 mm of the buttresses on either side of the HSS pinion by machining down to the nominal shaft diameter of 100 mm and counterboring a 25 mm diameter through hole. Other minor modifications allowed installation of a slip ring assembly on the upwind end of the shaft and radial holes to guide associated wiring.

2.2 Installation

Since the primary objective of Phase 3 testing of GB #2 is to measure high-speed shaft, pinion, and bearing loads, it is important to note two important differences between the gearbox drawings and the actual installation. These differences relate to the axial position of the high-speed shaft relative to the mating gear and CRB. Both of these items have been present since GB #2 was originally built prior to Phase 1 and Phase 2 testing, although they have only become relevant with the new instrumentation on the HSS in Phase 3. These two differences are:

- The baffle (P/N 251559) just upwind from the TRB pair shown in Figure 1 was never installed as part of the high-speed shaft assembly. The specified outer diameter of the

baffle is 180 mm; however, the measured minimum diameter of the housing cone is also 180 mm. When the gearbox was originally built, the baffle interfered with the housing and so it was removed from the HSS assembly. This process was simply repeated for Phase 3. The baffle is 5 mm thick, thus when omitted the TRB pair is 5 mm further upwind on the shaft itself.

- Upon installation of the instrumented high-speed shaft assembly into the gearbox in November 2013, it was noted that the counter bore inside the gearbox housing cone was deeper than specified in the drawings. The depth of the counter bore as specified in the rear housing (P/N 251342) was 254 mm; however, it was discovered that the depth is actually 260.8 mm. This counter bore depth was intended to locate the HSS assembly axially—that is, when the HSS assembly was inserted into the gearbox, it was intended to slide forward to the point at which the outer ring of the upwind TRB met the counter bore lip, leaving a 1-mm axial gap between the TRB spacer and the housing. With the counter bore being too deep, the HSS assembly was instead axially located by this latter feature. That is, the HSS assembly actually slid forward to the point at which the TRB spacer met the counter bore lip at 209 mm, leaving no axial gap. Thus, the entire HSS assembly is 1 mm further upwind than intended.

The net effects, relative to the published drawings, include the following:

- The TRB pair is located 1 mm further upwind relative to the housing and 5 mm further upwind relative to the HSS shaft. Furthermore, the upwind TRB is not restrained axially—there is a 5- to 6-mm axial gap between it and the housing.
- The HSS itself is 4 mm further downwind relative to the housing, resulting in two effects. First, the HS pinion is not centered on the HS gear by this amount, compared to the 120-mm facewidth of this mating gear pair. Second, the CRB rollers are offset from the shaft by 4 mm, compared to the 46 mm total width of the CRB. This offset tends to increase edge loading of the CRB rollers and CRB inner race. Visual confirmation by borescope revealed that the rollers are very close to the edge of the CRB inner race.

An illustration of these differences is shown in Figure 2. The gearbox designer was consulted regarding any implications relative to the gearbox operation. For short-term dynamometer testing, these slight differences were deemed to have a minimal impact; however, for detailed engineering analysis, especially the HS pinion facewidth load distribution and the HSS bending moments, these differences were deemed large enough to be accounted for in the gearbox models that are to be compared to the experimental data.

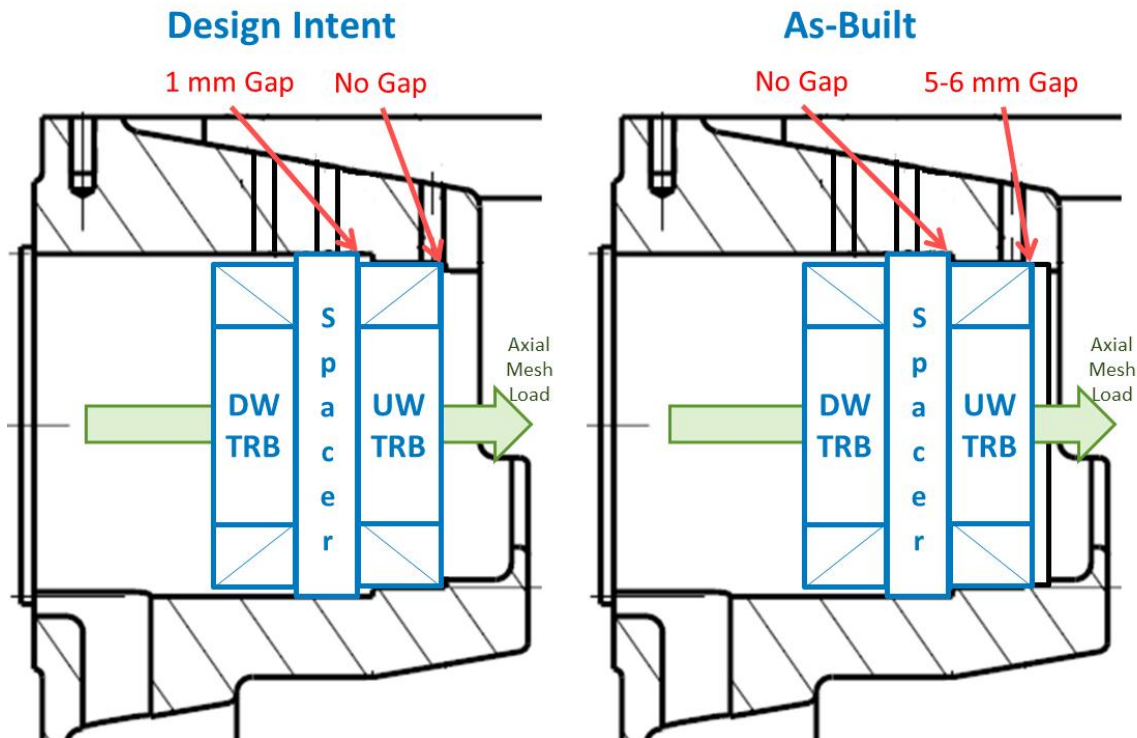


Figure 2. The effect of the deep counter bore in the HSS housing

2.3 Instrumentation

Table 1 lists the instrumentation that was installed on the HSS in April 2013. Eight uniaxial strain gauges are installed in the roots of the pinion teeth to measure the pinion face-width load distribution at locations shown in Figure 3. The axis of sensitivity of each gauge is perpendicular to the shaft axis, not the root fillet centerline. These gauges are arranged into two Wheatstone bridges to minimize the number of signals transmitted through the shaft-mounted slip ring assembly. The gauges are also spaced rotationally around the pinion to avoid active contact and signal response in adjacent Wheatstone bridge arms.

Additional sets of strain gauges are mounted in full bridge arrangements to measure two orthogonal shaft bending moments at each of three axial locations along the shaft along with shaft torque. These orthogonal moments allow for deriving the shaft moment vectors for subsequent use in determining TRB loads. The orthogonal moments are measured on either side of the HS gear mesh as shown in Figure 4 and Figure 5. These gauges are located at 88.5 mm (location B) and 260.5 mm (location A) from the upwind shaft end. A final set of strain gauges downwind of the TRB pair measures the orthogonal moments and the torque transmitted by the HSS as shown in Figure 6. These gauges are all located at 477 mm (location C) from the upwind shaft end. At all three locations the wiring was routed through radial holes into the shaft counterbore and then to the slip ring assembly. All wiring and gauges were covered for environmental protection. The instrumented shaft is shown in Figure 7 and Figure 8.

Table 1. HSS Instrumentation

| Part | Measurement | Label | Sensor(s) | Gauge Factor |
|----------------------------|-----------------------------------|--------------|-------------------------|---------------------|
| Pinion | Tooth Root Strain | HSP_K1234 | Vishay CEA-06-G1353-350 | 2.07 |
| Pinion | Tooth Root Strain | HSP_Kabcd | Vishay CEA-06-G1353-350 | 2.07 |
| Shaft, Upwind of Pinion | Shaft Bending Strain about Y-axis | HSS_UY_BM | Vishay CEA-06-125UN-350 | 2.11 |
| Shaft, Upwind of Pinion | Shaft Bending Strain about Z-axis | HSS_UZ_BM | Vishay CEA-06-125UN-350 | 2.11 |
| Shaft, Downwind of Pinion | Shaft Bending Strain about Y-axis | HSS_DY_BM | Vishay CEA-06-125UN-350 | 2.11 |
| Shaft, Downwind of Pinion | Shaft Bending Strain about Z-axis | HSS_DZ_BM | Vishay CEA-06-125UN-350 | 2.11 |
| Shaft, Downwind of Locknut | Shaft Bending Strain about Y-axis | HSS_exY_BM | Vishay CEA-06-125UN-350 | 2.11 |
| Shaft, Downwind of Locknut | Shaft Bending Strain about Z-axis | HSS_exZ_BM | Vishay CEA-06-125UN-350 | 2.11 |
| Shaft, Downwind of Locknut | Shaft Shear Strain | HSS_TQ | Vishay CEA-06-125UR-350 | 2.12 |

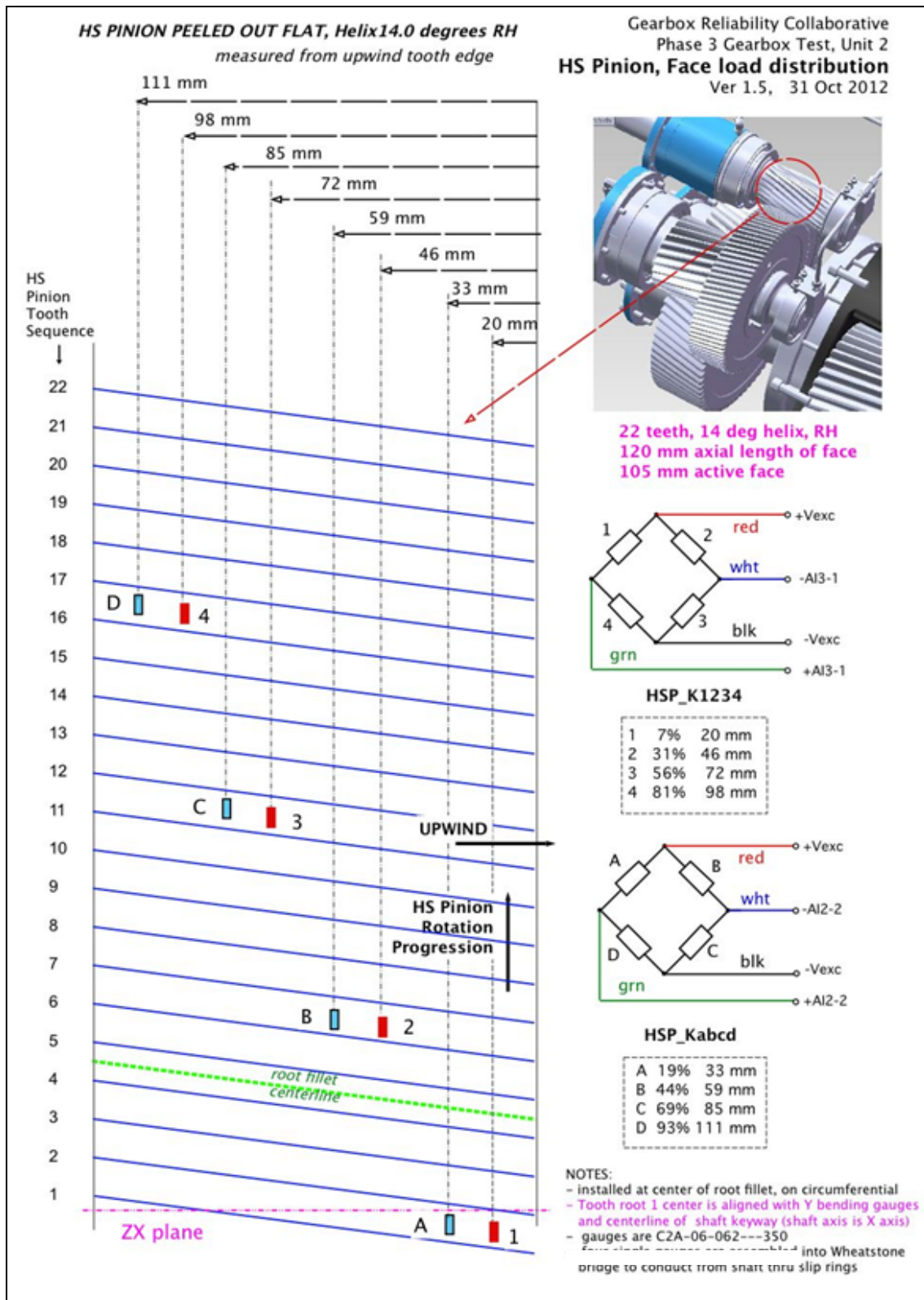


Figure 3. HSS pinion face width load distribution. *Illustration from McNiff Light Industry*

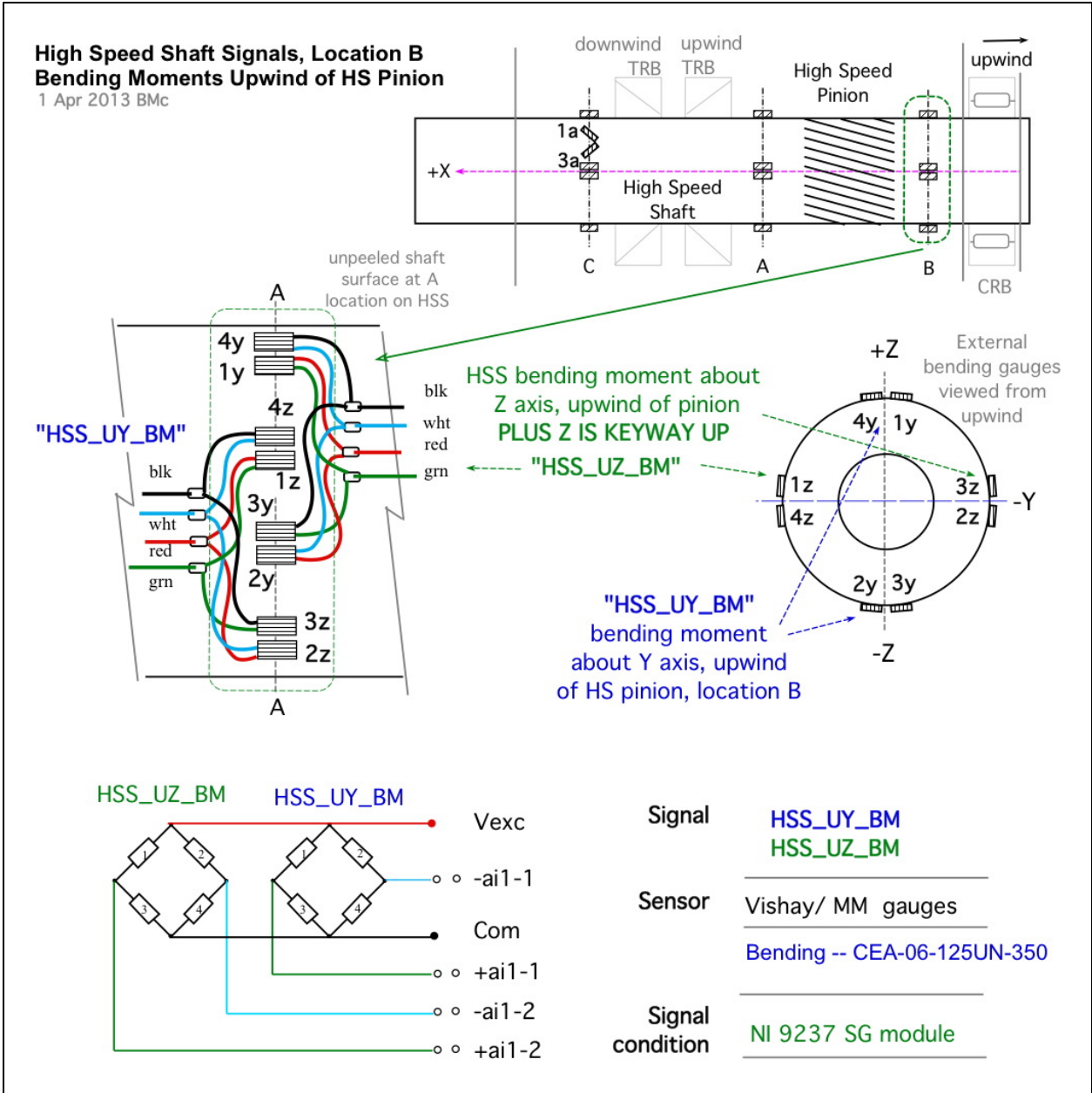


Figure 4. HSS bending upwind of the pinion. Illustration from McNiff Light Industry

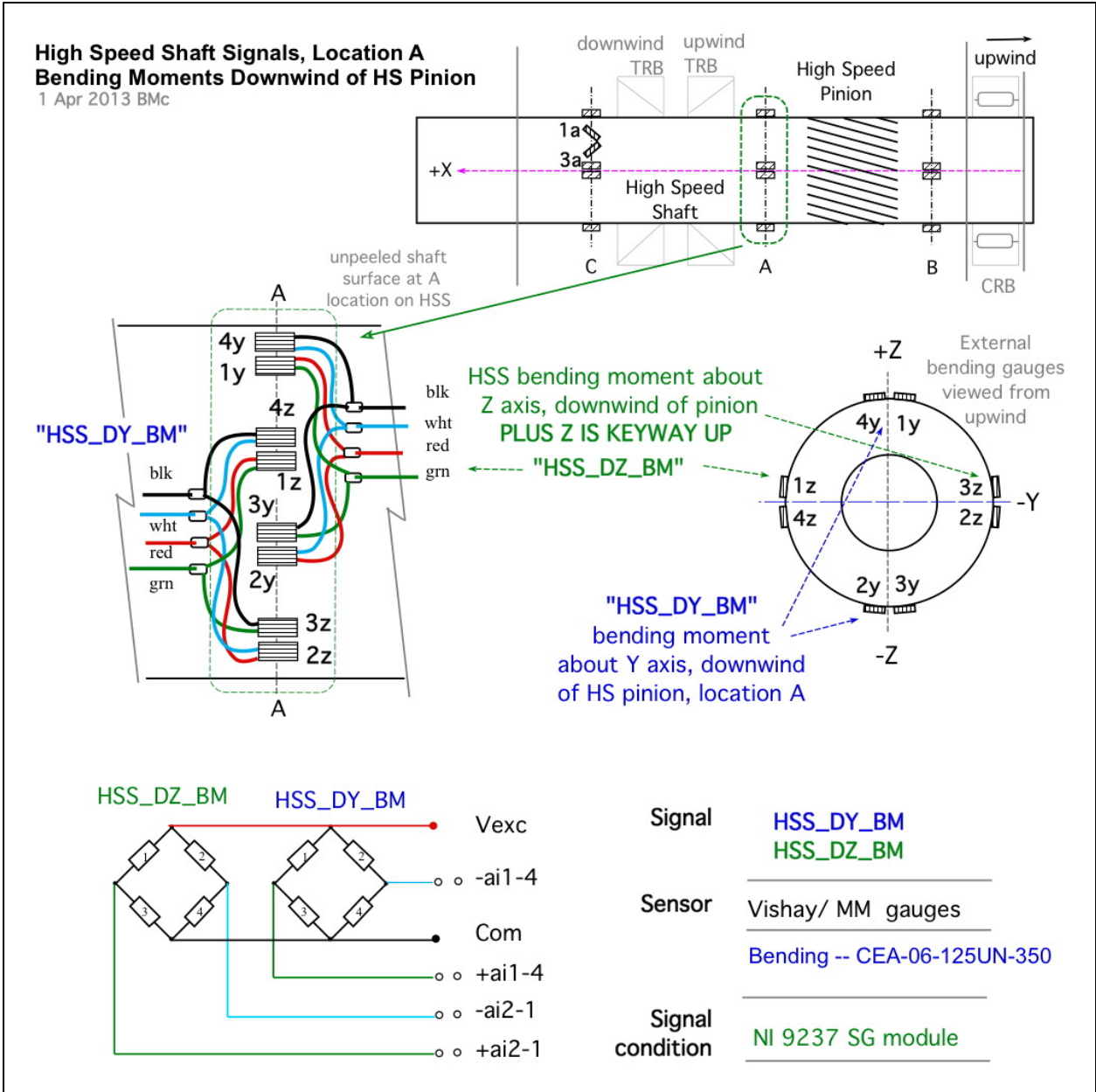


Figure 5. HSS bending downwind of the pinion. *Illustration from McNiff Light Industry*

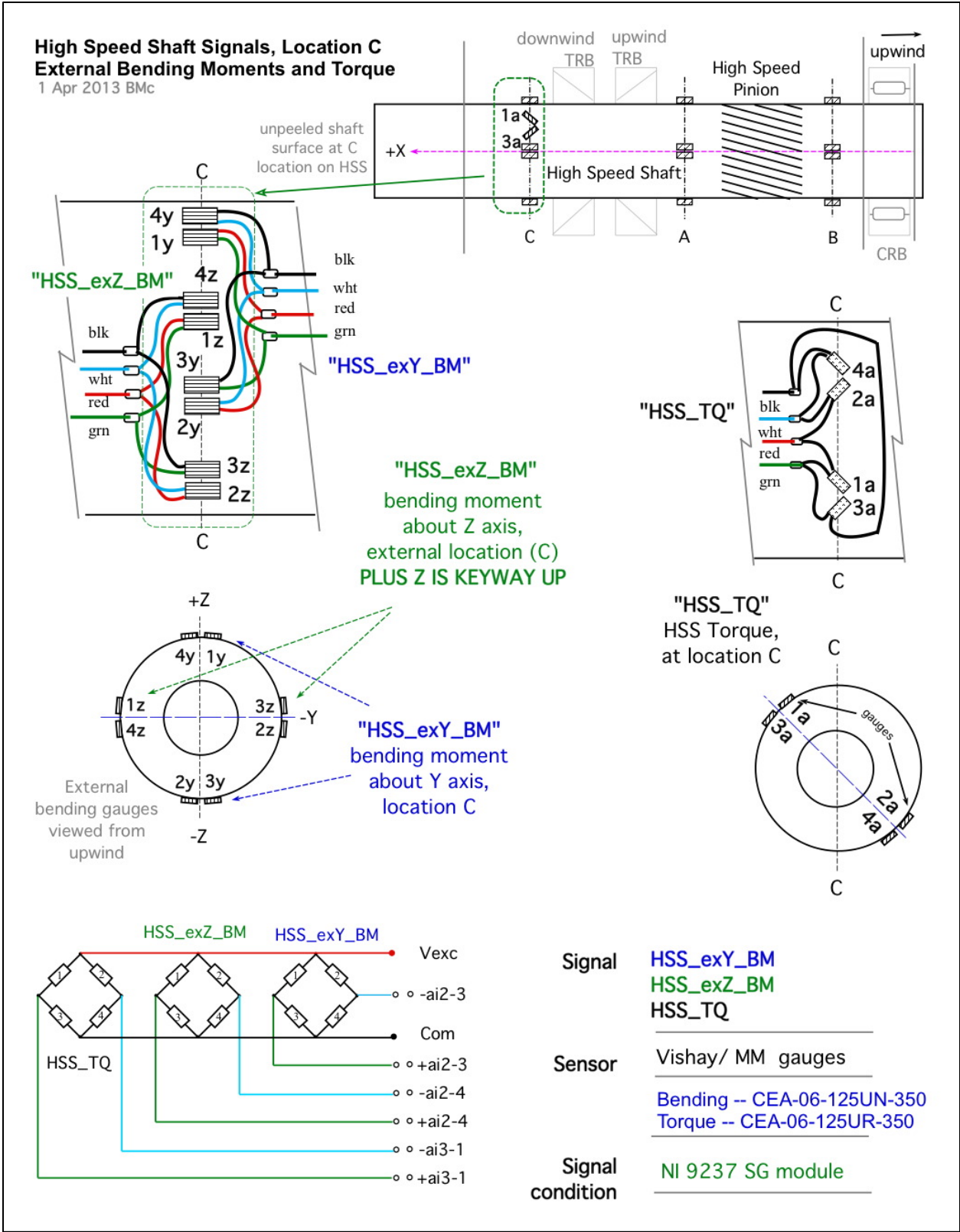


Figure 6. HSS bending and torque downwind of the TRB pair. Illustration by McNiff Light Industry

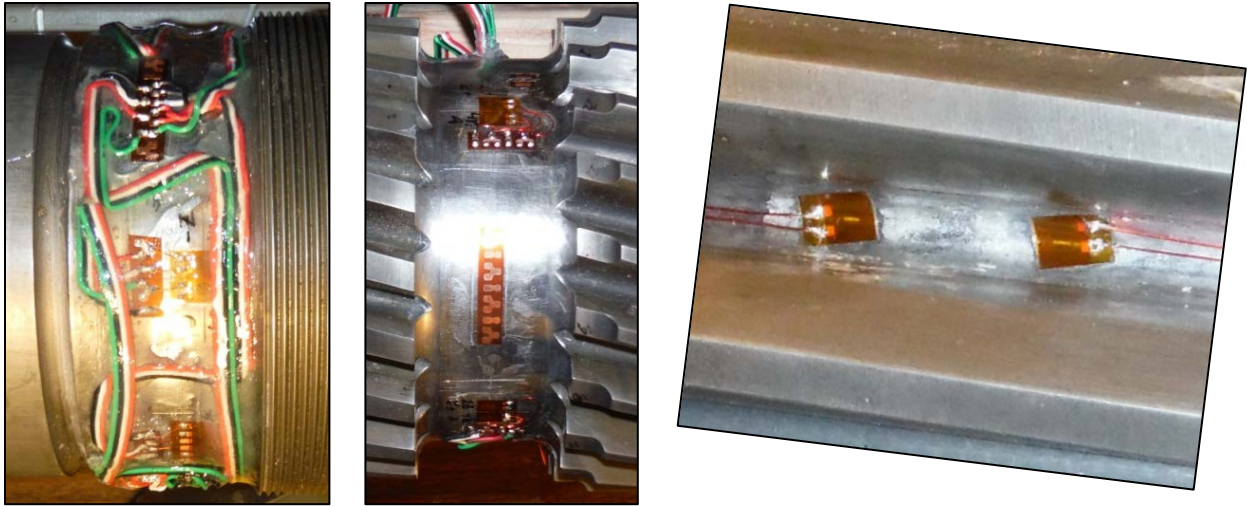


Figure 7. HSS torque, bending, and pinion strain gauges. Photos by Scott Naucner, NREL 30252, 30250, and 30251 (from left to right)



Figure 8. Instrumented HSS assembly. Photo by Jonathan Keller, NREL 27895

2.4 Calibration Requirements

The strain gauges installed on the pinion do not require calibration because only the relative difference between the gauges is used to determine the tooth face-width load distribution, not the absolute. The output from these strain gauges can simply be plotted with respect to each other, referencing them either to an observed maximum value or a predetermined nominal value.

In the case of the bending and torque strain gauges installed on the shaft itself, the absolute magnitude of load in kilonewton-meters (kNm) is of interest. The calibrations described in this report were carried out to accurately determine the relationship of the voltage output for these signals to engineering units with the proper sign or sense to the existing GRC coordinate system [4]. These measured loads can then be compared to predictions in the appropriate modeling software. Differences in the bending moment along the length of the shaft are especially of interest, because these moments are the primary cause of unequal load sharing in the TRB pair. Unequal load sharing between the TRB pair could be a leading cause of reliability issues in existing wind turbine gearboxes.

3 Test Configuration

3.1 Arrangement

The calibration test was performed in the high bay of the National Wind Technology Center (NWTC) 2.5-MW dynamometer. The HSS assembly was installed in GRC GB #2 in November 2013. This included installing the retaining end cap shown in Figure 1 and the hub of the brake disk (but not the brake disk itself or the generator coupling). This process of in situ calibration was expected to yield the most representative test results.

3.2 Load Application

An overhead crane was used along with a sling to pull upward with the calibration force, F_{cal} , on the end of the shaft at a distance of approximately 1 in. from the downwind end of the shaft. A spring scale was used to measure this applied load. In this manner, a bending moment, M_{cal} , was generated throughout the shaft. Positive and negative moments were applied to the y-axis and z-axis gauges by rotating the shaft 90 deg for each load application. For the purposes of this orientation, a permanent reference mark was made on the shaft. The mark is aligned with the positive z-axis as indicated in Figure 9. Note that in the case with the reference mark in the vertical positions (up or down), the resulting bending moment has the opposite sign of the applied force. In the case with the reference mark in the horizontal positions (port or starboard), the resulting moment has the same sign as the applied force.

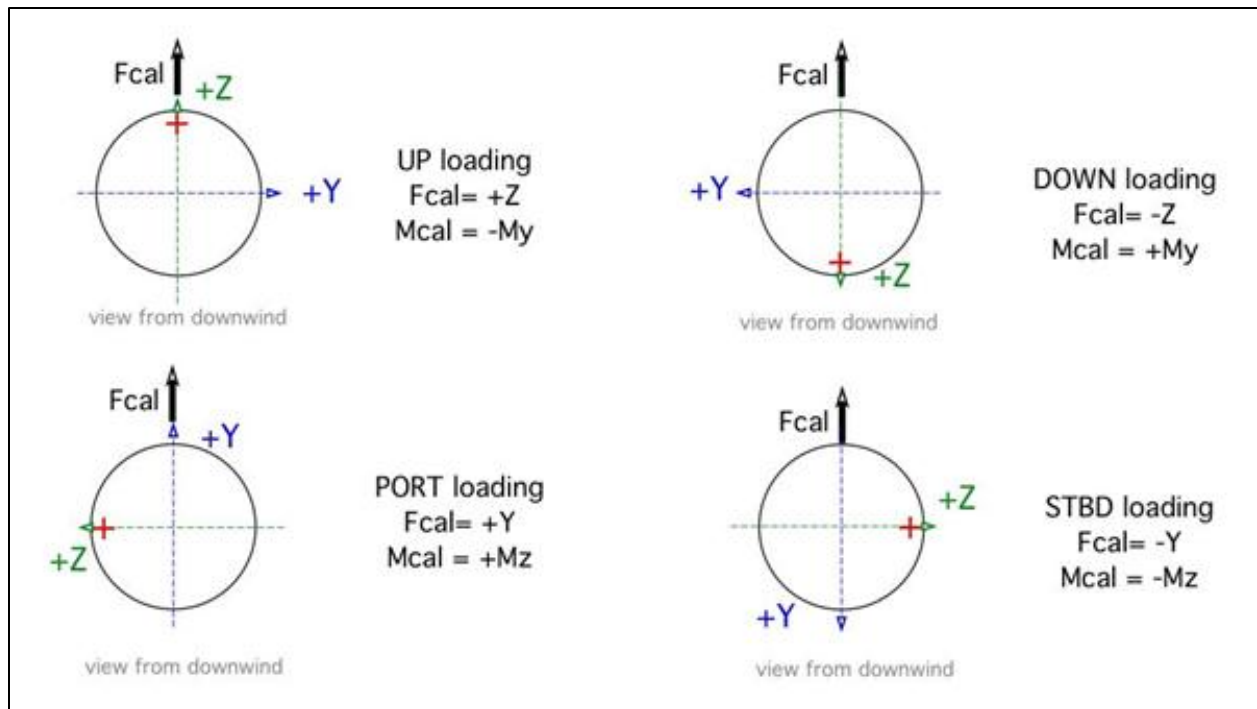


Figure 9. Shaft bending moment application. Illustration from McNiff Light Industry

Similarly, shaft torque was applied by wrapping the sling through an empty bolt hole in the brake disk hub on the port (left side when viewed from downwind) at a radius of approximately 6 in., as shown in Figure 10.

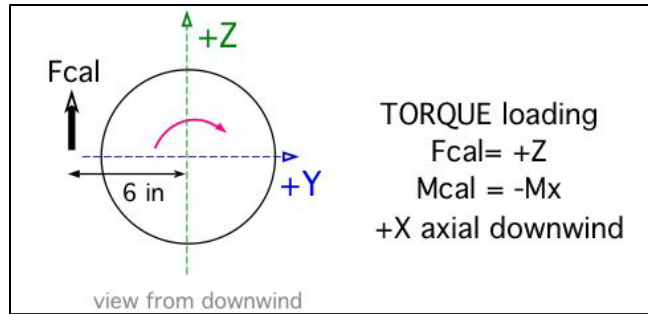


Figure 10. Shaft torque application. *Illustration from McNiff Light Industry*

3.3 Data Collection

The data acquisition system (DAS) used for the test is based on the National Instruments (NI) deterministic Ethernet platform. Three NI 9237 signal-conditioning modules collected the nine strain gauge bridges. The spring scale readings were recorded manually. All strain gauge channels for the calibration tests were recorded in native units of volts per volt (V/V); however, in subsequent dynamometer testing the units of record were changed to millivolts per volt (mV/V). For consistency, units of millivolts per volt are used for all graphs in this report. All the data channels were zeroed at the start of the test under no load with the reference mark on the shaft pointing up.

The data files for the bending moment tests were named using the convention “Ref_direction_load” where the direction corresponds to the direction in which the reference mark was facing (up, down, port, or starboard [STBD]). Each data file was also appended with “YYYY_MM_DD_HH_SS_ZZZHz.tdms,” where YYYY, MM, DD, HH, and SS are the year, month, date, hour, and second of the data acquisition; and ZZZ is the data acquisition rate in hertz (Hz). Only a single torque test was performed and it is simply labeled “Torque Sense.” All data were acquired at 100 Hz, although each test was static in nature.

4 Data Analysis

4.1 Response Verification

Because of the complex bridge wiring, it was important to verify that the signals responded as expected to a known applied load before the dynamometer testing started. The response of each bending signal to the applied force is shown in Figure 11 and Figure 12. In each figure, the response of the gauges to the resulting bending moments about their active axis and perpendicular to their active axis is shown. Examining the figures verifies that the moments responded as expected in several aspects. The gauges respond almost exclusively to moments about their active axis and with similar magnitudes, meaning that the response of the y-axis gauges to a y-axis moment is very similar to the response of the z-axis gauges to a z-axis moment. This was expected because the shaft section is an annulus at each bending gauge location. In addition, the gauges respond very little to a moment perpendicular to their active axis or torque. It is likely that any off-axis response may be caused by slight gauge orientation errors and any small error in the manual rotation of the shaft to the desired orientation during the test itself. Finally, as expected, the external gauges downwind of the locknut responded the most to the applied load. Conversely, the upwind gauges closest to the cylindrical roller bearing at the upwind end of the shaft responded the least. Corresponding to Figure 9, the y-axis response in Figure 11 has a negative slope. The z-axis response has a positive slope in Figure 12.

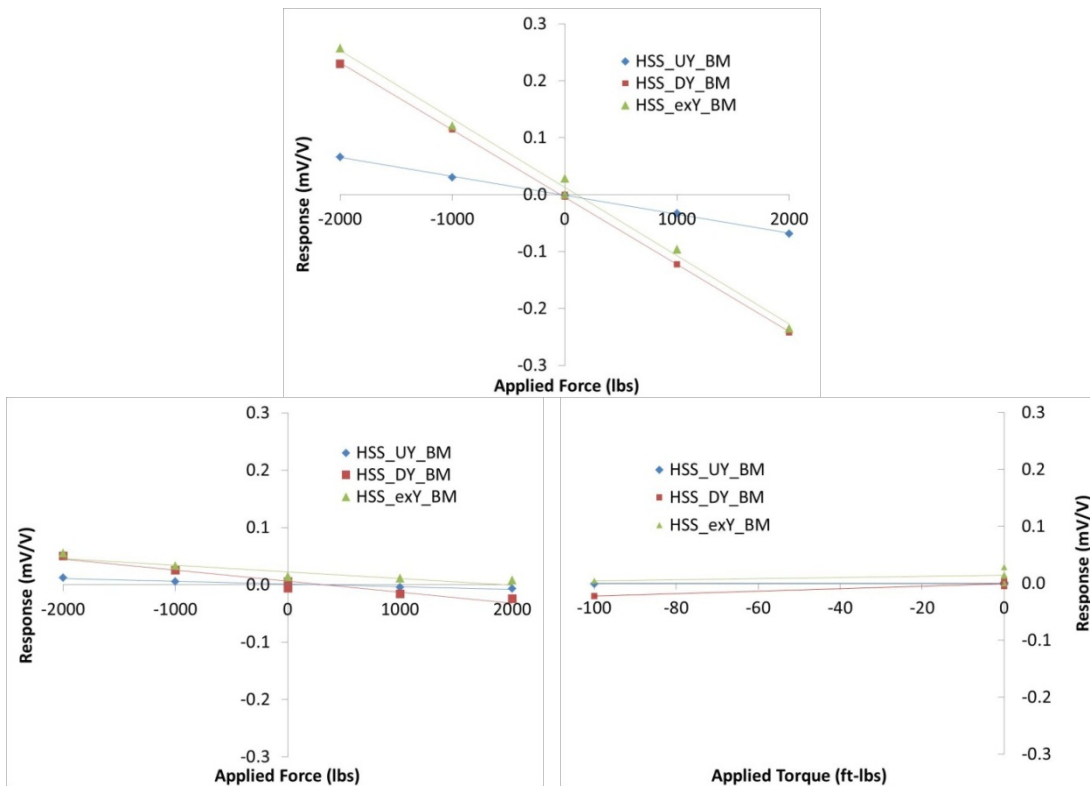


Figure 11. Y-axis gauge response to y-axis moment (top), z-axis moment (left) and torque (right)

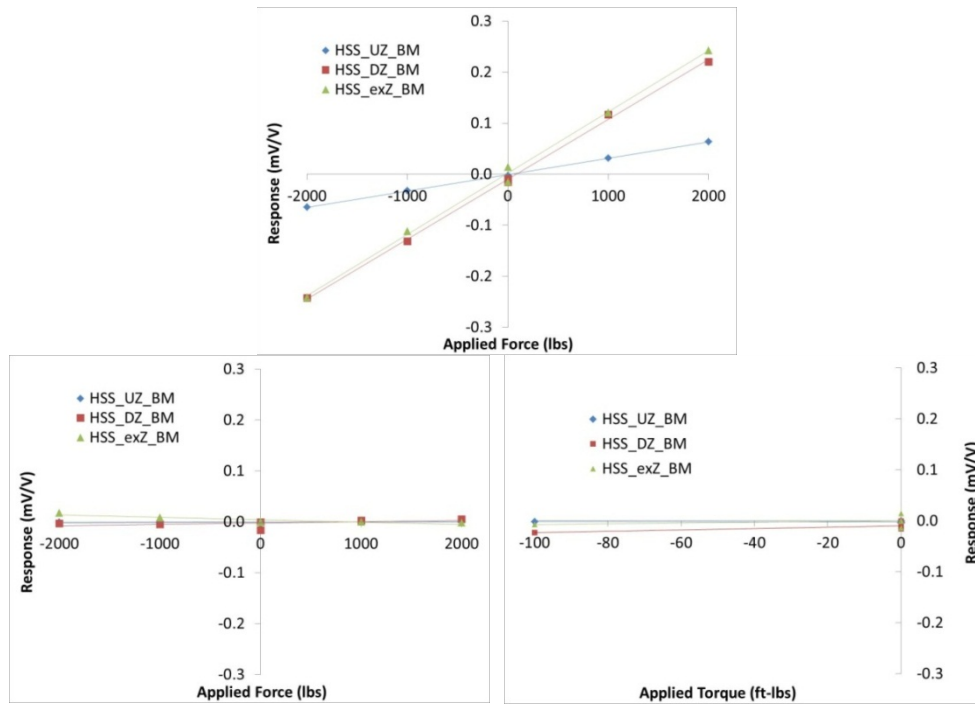


Figure 12. Z-axis gauge response to z-axis moment (top), y-axis moment (left), and torque (right)

The calibration equated to an applied torque of -100 foot-pounds (ft-lb) (-0.136 kNm), as shown in Figure 13. The HSS nominal torque is 4 kNm ($2,950$ ft-lb), so only a fraction of the rated torque was applied because of difficulties in restraining the system from rotating under load.

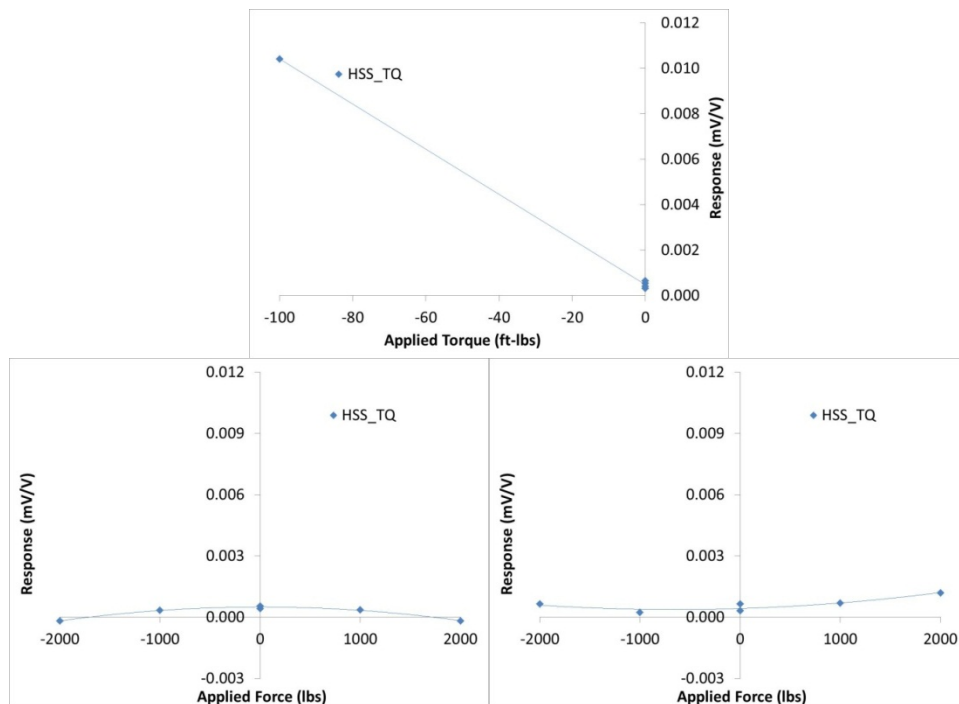


Figure 13. Torque gauge response to torque (top), to y-axis moment (left), and z-axis moment (right)

4.2 Calibration

Because the HSS cross section at the locations instrumented is simply an annulus, the relationships between measured strains and the resulting bending moment and torque can be determined from classical mechanics as described in this section. The resulting coefficients can then be used to convert the measured responses to engineering units.

4.2.1 Bending Moment Coefficient Derivation

For a circular shaft, the general relationship between bending moment and stress at the surface is

$$M = \sigma \frac{I}{D/2}. \quad (1)$$

The general relationship between stress and strain is

$$\sigma = \varepsilon E. \quad (2)$$

The area moment of inertia for an annulus is

$$I = \frac{\pi(D^4 - d^4)}{64}. \quad (3)$$

Substituting equations (2) and (3) into (1) yields

$$M = \frac{\pi(D^4 - d^4)E}{32D} \varepsilon. \quad (4)$$

The relationship between the bending strain gauge output and the bending strain itself is [5]

$$\frac{dV}{V} = G_f \varepsilon. \quad (5)$$

The relationship between the bending moment and strain gauge output, then, is

$$M = \frac{\pi(D^4 - d^4)E}{32DG_f} \frac{dV}{V} = K_M \frac{dV}{V}. \quad (6)$$

4.2.2 Torque Coefficient Derivation

For a circular shaft, the general relationship between torque and shear stress at the surface is

$$T = \tau \frac{J}{D/2}. \quad (7)$$

The general relationship between shear stress and shear strain is

$$\tau = \gamma G. \quad (8)$$

The relationship between the shear modulus and the elastic modulus is

$$G = \frac{E}{2(1+\nu)}. \quad (9)$$

The polar moment of inertia for an annulus is

$$J = \frac{\pi(D^4 - d^4)}{32}. \quad (10)$$

Substituting equations (8) through (10) into equation (7) yields

$$T = \frac{\pi(D^4 - d^4)E}{32D(1+\nu)}\gamma. \quad (11)$$

In this configuration of the torque bridge, the relationship between the torque strain gauge output and the shear strain itself is [5]

$$\frac{dV}{V} = \frac{1}{2}G_f\gamma. \quad (12)$$

The relationship between the bending moment and strain gauge output, then, is

$$T = \frac{\pi(D^4 - d^4)E}{16DG_f(1+\nu)}\frac{dV}{V} = K_T\frac{dV}{V}. \quad (13)$$

4.2.3 HSS Calibration Coefficients

The HSS material properties and dimensions, along with the resulting calibration coefficients K_M and K_T , are listed in Table 2. Refer to Table 1 for the strain gauge factors.

Table 2. HSS Properties

| Inner Diameter | Outer Diameter | Modulus of Elasticity | Poisson's Ratio | Bending Moment Coefficient | Torque Coefficient |
|----------------|----------------|-----------------------|-----------------|----------------------------|--------------------|
| d | D | E | ν | K_M | K_T |
| (m) | (m) | (GPa) | | (kNm) | (kNm) |
| 0.025 | 0.1 | 207 | 0.3 | 9594 | 14690 |

4.2.4 Calibration Results

Applying the calculated bending coefficient to the measured signal responses yields a semianalytic bending moment measurement. Plotting the resulting bending moment versus shaft position then results in the classical bending moment diagram shown in Figure 14. In this figure, the result is plotted regardless of sign or shaft orientation to present a condensed view. In an effort to verify that the determined bending coefficient yields accurate results, the semianalytic bending moments were also compared to those predicted by classical mechanics and

RomaxWind software. For the classical shear-moment (V-M) mechanics, it was assumed that the TRBs only reacted with point loads that neutralize the moment from the applied force. The GRC model in RomaxWind software was modified to remove the generator coupling and include the applied calibration force in a static condition. Each method assumes that the bearings react a force or moment at their midpoint.

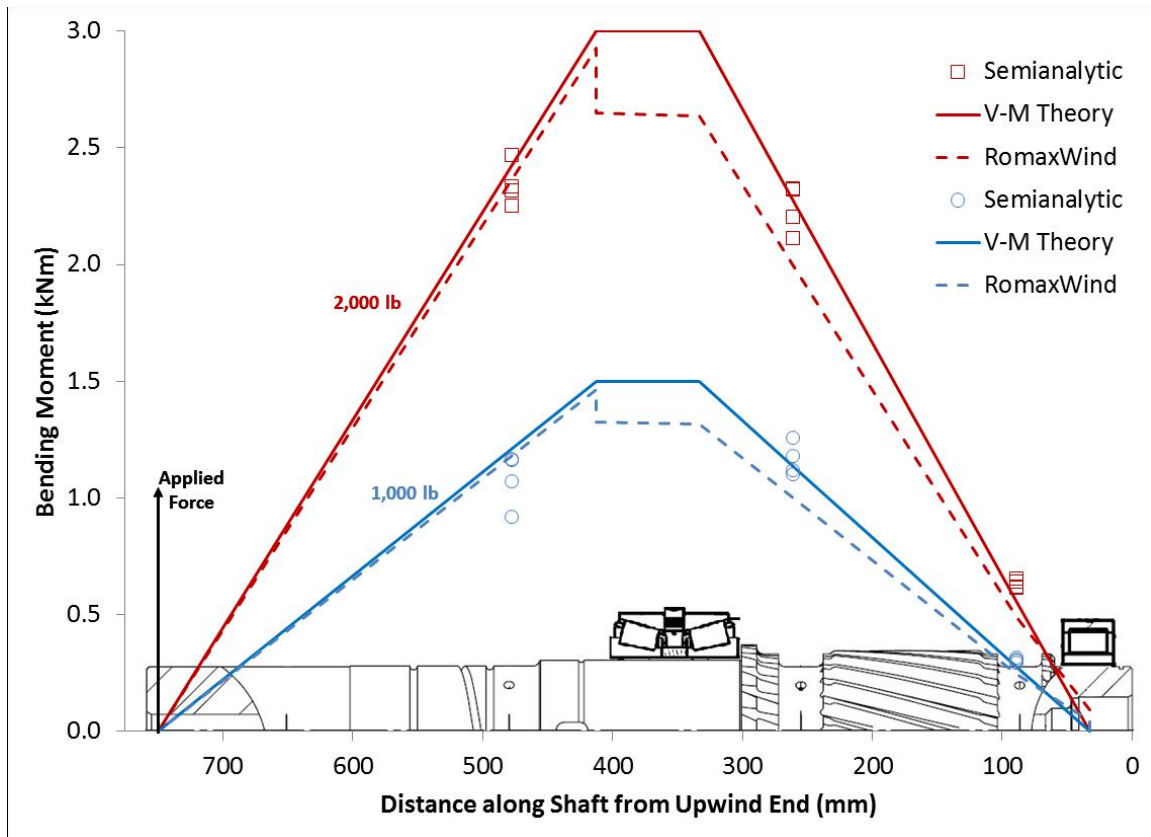


Figure 14. Bending moment diagram

There is generally very good agreement between the measured data and the models. The largest difference results from the RomaxWind model predicting small point moments applied by the downwind TRB and the CRB, which are likely a result of the bearing microgeometries and settings. It is interesting to note that the measured moment just upwind of the TRB pair is almost as large as just downwind of the TRB pair. This is somewhat counterintuitive, because as mentioned earlier, the TRB pair is in a “stiff” O-configuration. A “very stiff” TRB pair would essentially act as a cantilever, completely reacting the moment from the applied force and resulting in no moment at all in the portion of the shaft between the TRB and CRB. Clearly, the TRB pair has some tilting flexibility, which allows the moments to continue in that section of the shaft.

Because the torque is only applied and measured in one place, there is no need for a diagram. The applied torque was approximately 0.14 kNm; the semianalytic calculated torque was 0.15 kNm. Although this is a difference of approximately 10%, it is deemed sufficient correlation because of the difficulties in measuring the exact moment arm in addition to the accuracy of the weight scale.

4.3 Final Calibration Coefficients

As stated in the introduction, the purpose of this document is to describe this calibration process and the test results in such a way that the raw signal information gathered during subsequent dynamometer testing can be related to measured shaft bending and torque. This section describes how the raw dynamometer data can be converted to engineering units.

Recall that all strain gauge channels for the calibration tests discussed in this report were actually recorded in native units of volts per volt of excitation and the data channels were zeroed at the start of the test with only the brake disk hub installed. As demonstrated in Figure 11 through Figure 13, when no force is applied, the strain gauge response is almost zero. True zeroes are very difficult to achieve because the shaft weight and brake disk hub weight result in a moment. The gauge response to this moment can be zeroed for any given shaft position, but as soon as the shaft is rotated to another orientation, the measured gauge response will no longer be zero.

In subsequent dynamometer testing, however, these two conditions changed. Most importantly, the units of record for these channels were changed to millivolts per volt to match the units for the existing strain gauge channels for the remainder of the gearbox. In addition, the brake disk and generator coupling were installed. These components, weighing more than 100 kg (220 lb) combined, create additional moments that were not accounted for in the original zeroing process. Through both effects, an unintentional offset was introduced to the dynamometer test data. This section describes the process for removing this unintentional offset.

Table 3 lists the scaling factors and offsets that should be applied to the dynamometer test data to convert those data to engineering units of interest. For each data channel, the equation takes the following form:

$$y = mx + b, \tag{14}$$

where y is the processed data in engineering units and x is the signal output (in units of millivolts per volt) as recorded in the dynamometer testing. Shaft torque is typically expressed as a positive quantity, so the negative slope in Figure 13 was ignored.

Table 3. Final HSS Calibration Coefficients

| Label | Scale Factor <i>m</i> (kNm/mV/V) | Offset <i>b</i> (kNm) |
|------------|--|-----------------------------|
| HSS_UY_BM | -9.594 | 1.756 |
| HSS_UZ_BM | 9.594 | -5.372 |
| HSS_DY_BM | -9.594 | -2.875 |
| HSS_DZ_BM | 9.594 | -7.346 |
| HSS_exY_BM | -9.594 | -7.902 |
| HSS_exZ_BM | 9.594 | 4.418 |
| HSS_TQ | 14.690 | -1.086 |

For the bending moments, the final offset b was determined from an average of five dynamometer test data sets when the gearbox was operating at full speed and power settings were ranging from offline to 100% rated power (750 kW) in increments of 25% power. When these offsets are applied to the dynamometer test data, the resulting bending moments have no mean value, as expected. This method of determining the offset was deemed the most representative because it accounts—to the maximum extent possible—for the bending moment resulting from the brake disk and generator coupling. It is noteworthy that if the offset b is instead determined by accounting for the scale factor and unit conversion of the original offsets shown in Figure 11 and Figure 12, the result closely approximates the offset listed in Table 3 (typically within 5%). For the torque, the final offset was determined by simply accounting for the scale factor and unit conversion of the original offset shown in Figure 13.

As a final check, the initial dynamometer test data sets were converted using the coefficients in Table 3. These are shown in Figure 15 and Figure 16. For clarity, the data are plotted with respect to the shaft azimuth and 10 revolutions of the shaft are shown. As noted earlier, the mean value for each bending moment is approximately zero, as expected. In addition, the data from revolution to revolution are repeatable. The bending moments on either side of the pinion are strongly affected by power; the bending moment downwind of the TRB pair, however, changes only slightly with power. The latter is expected because the gear mesh loads are largely reacted by the TRB pair and the CRB.

The torque shows a strong, linear correlation with power, as expected. A final check can be made here as well—when the drivetrain is operating at 100% power (750 kW electrical power) the theoretical main shaft torque is 324 kNm assuming no losses. Dividing by the gearbox ratio of 81.49 yields a theoretical HSS torque of 4 kNm. The average measured torque is 4.2 kNm, which is slightly higher than theoretical because of efficiency losses.

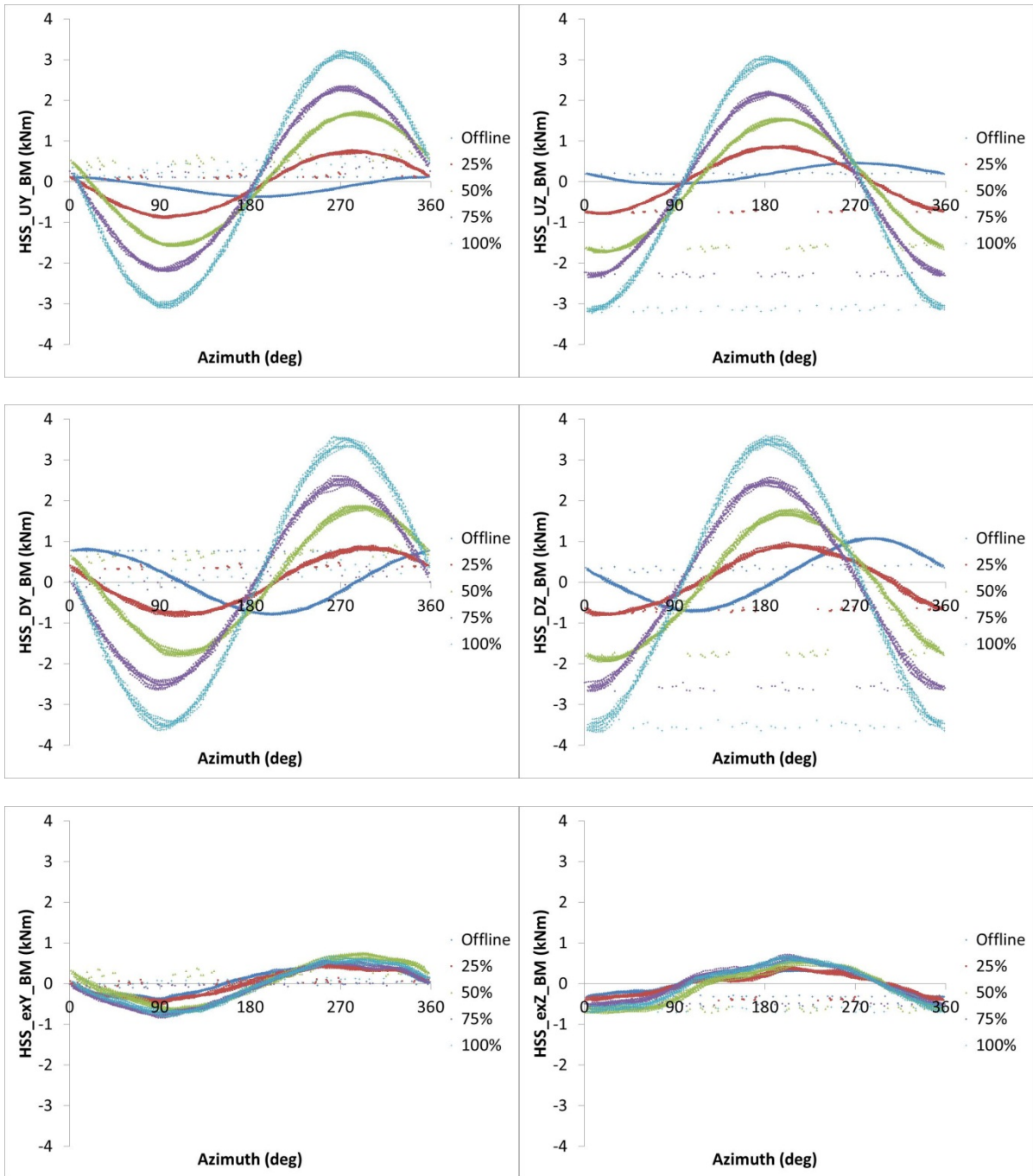


Figure 15. Measured bending moments in dynamometer test

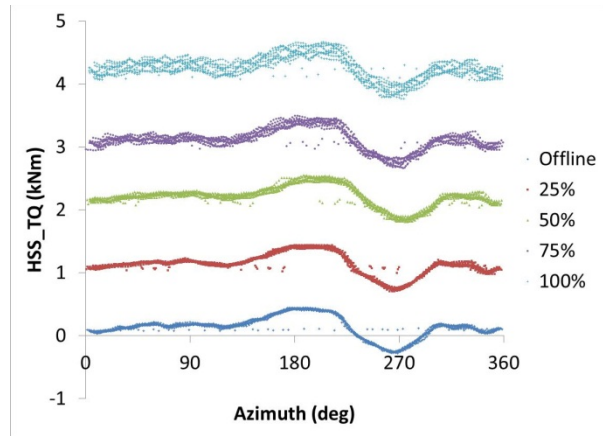


Figure 16. Measured torque in dynamometer test

5 Conclusions

An instrumentation package was designed, installed, and calibrated for the GRC gearbox HSS pinion and shaft. The instrumentation consists of nine strain gauge bridges installed to measure face-width load distribution, shaft bending moments, and torque. The bending moment and torque strain gauges underwent in situ calibration testing on November 26, 2013, in the 2.5-MW dynamometer high bay at the NWTC. The final calibration coefficients were determined so that each quantity could be converted from the recorded raw signal to engineering units.

The measured bending moments and torque signals were compared to classical theory and the GRC RomaxWind model. Sample dynamometer test data sets were also examined to check the quality of the data and determine required offsets. The results can be summarized as follows:

- The measured bending moments in the static calibration tests match very closely to those calculated using classical mechanics and the GRC RomaxWind model. The measured torque also matches very closely to classical mechanics.
- Very little cross-coupling exists between the y- and z-axis bending moment strain gauges.
- The measured bending moments from initial dynamometer tests exhibit the expected signal behavior. Shaft bending moments on either side of the HSS pinion and shaft torque have strong, linear correlations with power. The shaft bending moment downwind of the TRB pair is also unaffected by power.
- The measured shaft torque also compares favorably to the expected torque at rated power.

Publications examining this instrumentation set and their comparison to common software tools can now be written in terms of equivalent engineering units.

6 References

1. Link, H.; LaCava, W.; van Dam, J.; McNiff, B.; Sheng, S.; Wallen, R.; McDade, M.; Lambert, S.; Butterfield, S.; Oyague, F. *Gearbox Reliability Collaborative Project Report: Findings from Phase 1 and Phase 2 Testing*. NREL/TP-5000-51885. Golden, CO: NREL, 2011.
2. van Dam, J. *Gearbox Reliability Collaborative Bearing Calibration*. NREL/TP-5000-47852. Golden, CO: NREL, 2011.
3. Keller, J.; Guo, Y.; McNiff, B. *Gearbox Reliability Collaborative High Speed Shaft Tapered Roller Bearing Calibration*. NREL/TP-5000-60319. Golden, CO: NREL, 2013.
4. Sheng, S. “Report on Wind Turbine Subsystem Reliability—A Survey of Various Databases.” NREL/PR-5000-59111. Golden, CO: NREL, 2013.
5. Link, H.; Keller, J.; Guo, Y.; McNiff, B. *Gearbox Reliability Collaborative Phase 3 Gearbox 2 Test Plan*. NREL/TP-5000-58190. Golden, CO: NREL, 2013.
6. Vishay Precision Group. *Strain Gage Rosettes: Selection, Application and Data Reduction*. Tech Note TN-515. Malvern, PA: Vishay Precision Group, 2010. Accessed July 16, 2014: <http://www.vishaypg.com/docs/11065/tn-515.pdf>.